

A constraint multi-objective evolutionary optimization of a state-of-the-art dew point cooler using digital twins

 The corrections made in this section will be reviewed and approved by a journal production editor.

Yousef **Golizadeh Akhlaghi** Writing - review & editing Writing - original draft Investigation
Conceptualization ^a, Ali **Badiei** Writing - original draft Investigation ^a, Xudong **Zhao** Funding acquisition
Project administration ^{a,*} Xudong.Zhao@hull.ac.uk, Koorosh **Aslansefat** Conceptualization Investigation
Writing - review & editing ^b, Xin **Xiao** Conceptualization Investigation Writing - review & editing ^{a,*}
X.Xiao@hull.ac.uk, Samson **Shittu** Investigation ^a, Xiaoli **Ma** Supervision ^a

^aCentre for Sustainable Energy Technologies, Energy and Environment Institute, University of Hull, Hull
HU6 7RX, UK

^bDepartment of Computer Science, University of Hull, Hull HU6 7RX, UK

*Corresponding authors.

Abstract

This study is pioneered in developing digital twins using Feed-forward Neural Network (FFNN) and multi objective evolutionary optimization (MOEO) using Genetic Algorithm (GA) for a counter-flow Dew Point Cooler with a novel Guideless Irregular Heat and Mass Exchanger (GIDPC). The digital twins, takes the intake air characteristics, i.e., temperature, relative humidity as well as main operating and design parameters, i.e., intake air velocity, working air fraction, height of HMX, channel gap, and number of layers as the inputs. GIDPC's cooling capacity, coefficient of performance (COP), dew point efficiency, wet-bulb efficiency, supply air temperature and surface area of the layers are selected as outputs. The optimum values of aforementioned operating and design parameters are identified by the MOEO to maximise the cooling capacity, COP, wet-bulb efficiencies and to minimise the surface area of the layers in four identified climates within Köppen-Geiger climate classification, namely: tropical rainforest, arid, Mediterranean hot summer and hot summer continental climates. The system monthly and annual performances in the identified optimum conditions are compared with the base system and the results show the annual improvements of up to 72.75% in COP and 23.57% in surface area. In addition, the annual power

consumption is reduced by up to 49.41% when the system is designed and operated optimally. It is concluded that identifying the optimum conditions for the GIDPC can increase the system performance substantially.

Keywords: Dew point cooler; Genetic algorithm; Multi objective evolutionary optimization; Neural network; Digital twins

Nomenclature

A	area, m ²
C _p	specific heat capacity, kJ/(kg°C)
COP	coefficient of performance
dp	dew point
D _h	hydraulic diameter, m
D _e	Equivalent diameter, m
en	Latent heat, kJ/kg
G	channel gap, m
h	convection coefficient, W/(m ² °C)
h _m	mass transfer coefficient, m/s
H	channel height, m
hum	humidity ratio, kg/kg
i	enthalpy, kJ/kg
Le	Lewis number
Nu	Nusselt number
N _L	number of layers
P	pressure, Pa
Q _{cooling}	cooling capacity, W
Q	heat transfer, W
Q _m	mass flow rate, kg/s
Re	Reynolds number
RH	relative humidity
T	temperature, °C
U	air velocity, m/s
W	electric power, kW

Subscripts

Subscripts

air	air
dp	dew point
dry	dry channel

fan	fan
in	inlet
out	outlet
pump	pump
s	surface
steam	water steam
vap	evaporated water
water	water
wet	wet channel
w	wall
wb	wet bulb

Greek symbols

Greek symbols

λ	Thermal conduction coefficient, kW/(m °C)
σ	surface wettability factor
φ	working air fraction over the intake air
ε	efficiency
ρ	density, kg/m ³
Le	Lewis number
Δ	difference between two states
λ_f	coefficient of friction resistance
ξ	coefficient of local resistance

Abbreviations

Abbreviations

COP	Coefficient of Performance
DPEGIDPC	Guideless Irregular Dew Point Cooler
IEC	Indirect Evaporative Cooling
MVC	Mechanical Vapor Compression
MSE	Mean Square Error
GA	Genetic Algorithm
MOEO	Multi Objective Evolutionary Optimization
FFNN	Feed-Forward Neural Network

1 Introduction

1.1 Background

To provide comfortable indoor air quality, air conditioners are needed in modern buildings but astronomical part of the energy supplied to buildings, i.e., up to 50% [1], is consumed by air conditioner systems. Energy intensiveness of the conventional Mechanical Vapor Compression (MVC) air conditioners [2], has led the researchers toward an efficient replacement [3]. Evaporative cooling system, with direct **evaporative cooling** (DEC) and **Indirect evaporative cooling** (IEC) types, were introduced as an environmentally friendly cooling systems in the past decades [2,4,5]. The IECs are more preferred owing to their superiority in keeping the humidity within the acceptable levels [6,7]. Necessity of inventing more efficient cooling systems resulted in introducing the Dew Point Coolers (DPCs) by a remarkable potential in cooling down the intake air temperature to its dew point temperature [8,9]. The M-cycle Heat and Mass Exchanger (HMX) was the core initiative of this technology which caused a significant decrease in dew point and wet-bulb temperatures of the air in the wet channel leading to up to 30% higher cooling efficiency [10] with two main types: cross flow and counter-flow [11].

1.2 Literature review: dew point cooler

The first ever research was done in Coolerado® project in USA [10] where a cross flow DPC reached wet-bulb and dew-point efficiencies of 80% and 50%, respectively. Zhao et al. [12] identified that the northern and west regions of China were the suitable regions for DPC operation. Rianguilaikul and Kumar [13] experimentally, concluded that the wet-bulb and dew point efficiencies of a DPC were in the range of 92–114%, and 58–84%, respectively. Bruno [14] investigated the applicability of a DPC prototype in both commercial and residential buildings. Jradi et al. [15] achieved wet-bulb efficiencies of 70–117% with supply air flow rate of 300–1500 m³.h⁻¹ in a cross-flow DPC. Pandelidis et al. [16] studied the effect of the inlet air parameters on performance of HMXs in different types of M-Cycle systems. Lin et al. [17] concluded that the saturation point of the working air is regardless of the intake air conditions. Xu et al. [18] conducted two studies by introducing a novel super performance DPC with 30–60% higher performance. It is also reported that the COP of the proposed system can reach 52.5 at the ideal operating condition with working air ratio of 0.36 [19]. In an experimental study, Lin et al. [20] found that the performance of the selected cross flow DPC was negatively affected by the wet conditions. The exergy flow and efficiency ratio of the cross flow DPC under various conditions [21], and the effect of sprayed water in the wet channel of a counter-flow DPC [22] were investigated. Other studies [23,24] were also carried out in which the key governing dimensionless numbers and correlations for the transient and steady-state characteristics were proposed. Wan et al. [25] selected two DPCs with two different air flow configurations and compared cooling effectiveness and product temperature of both types. A thermodynamic analysis on a hybrid membrane liquid desiccant dehumidification and DPC was done in which the targeted supply air temperature of 20.0–28.0 °C with the humidity ratio less than 12.0 g/kg were reached [26]. Wan et al. [27] calculated the heat and mass coefficients in a counter-flow DPC with the NTU-Le-R method with maximum discrepancies of 6%. Liu et al. [28] reported the wet-bulb efficiency and COP improvements of a counter-flow DPC by 29.3% and 34.6% respectively, compared with the commercial DPCs. In addition, Liu et al. [29] identified the best operating conditions for the selected counter-flow DPC.

1.3 Artificial Intelligence in DPC, and the identified gap

Over the past decade, Artificial Intelligence (AI) is brought into the DPC technology which has led to outstanding results for performance prediction and optimum operation of DPCs. Pandelidis and Anisimov [30] used Response Surface Methodology (RSM) for a cross-flow M-cycle heat exchanger. It was concluded that performance of the system was mainly affected by supply air mass flow rate, inlet air temperature and relative humidity. Sohani et al. [31] used the Group Method of Data Handling-type neural network (GMDH) and Multi Objective Optimization (MOO) methods to predict the supply air properties and optimize the performance of a cross flow DPC. It was concluded that the COP and cooling capacity were improved by 8.1% and 6.9% respectively. Jafarian et al. [32] also used the same method for a counter-flow DPC, which could predict the supply air temperature. In addition, using MOO, COP and specific area of the cooler were optimized. Sohani et al. [33] compared the performance of the counter-regenerative and cross flow DPCs after identifying their optimum operating conditions. As a result, the proper climate for each DPC was introduced. Sohani et al. [34] also presented an hourly optimizations method for the DPCs employing the MOO. Pakari and Ghani [35] used the regression models to predict the performance of a counter-flow DPC. An optimization based study [36] revealed that the optimal channel length and working ratio for the considered DPC were 0.50 m and 0.40 respectively.

Review of the existing literature revealed that the studies on DPCs have been mostly concentrated on the commercial HMXs. However, a novel counter-flow GIDPC has the best performance in terms of COP value i.e., 52.5 [18,19]. Xu et al. [18] pioneered in introducing the GIDPC through the numerical and experimental studies [19], and Akhlaghi et al. [37] proposed a data-driven model which was based on the Multiple Polynomial Regression (MPR). However, to date, no optimization algorithm, considering both operating and design parameters, is developed for the GIDPC. Thus, the lack of a robust AI model which can identify the optimum operating and design parameters of the GIDPC in diverse climates is identified as an outstanding gap for the state-of-the-art DPC. Identification of the dedicated optimum parameters in each climate, will reduce the construction cost and improve the GIDPC efficiency in terms of power consumption and cooling performance.

Therefore, this study is pioneered in proposing a constraint multi objective evolutionary optimization (MOEO) and digital twins for GIDPCs. The digital twins is developed using Feed-forward Neural Network (FFNN) method, and the MOEO is developed based on the Genetic Algorithm (GA) to, firstly, predict the performance of the system in any random operating condition using a big dataset and, secondly, to identify the optimum values of the operating and design parameters in diverse climates. A validated numerical model is used to construct a big dataset for training the FFNN model. The input parameters of the dataset include main operating parameters, i.e., temperature, relative humidity and velocity of the intake air, and key design parameters, i.e., working air fraction, HMX height and channel gap, and number of layers in HMX structure. Having developed the digital twins, the MOEO is used to find the optimum operating and design parameters to maximise the cooling capacity, COP, wet-bulb efficiency and to minimise the surface area of the layers, as the objectives of the MOEO, in four suitable climates for GIDPC operation based on the Koppen–Geiger’s classification [38].

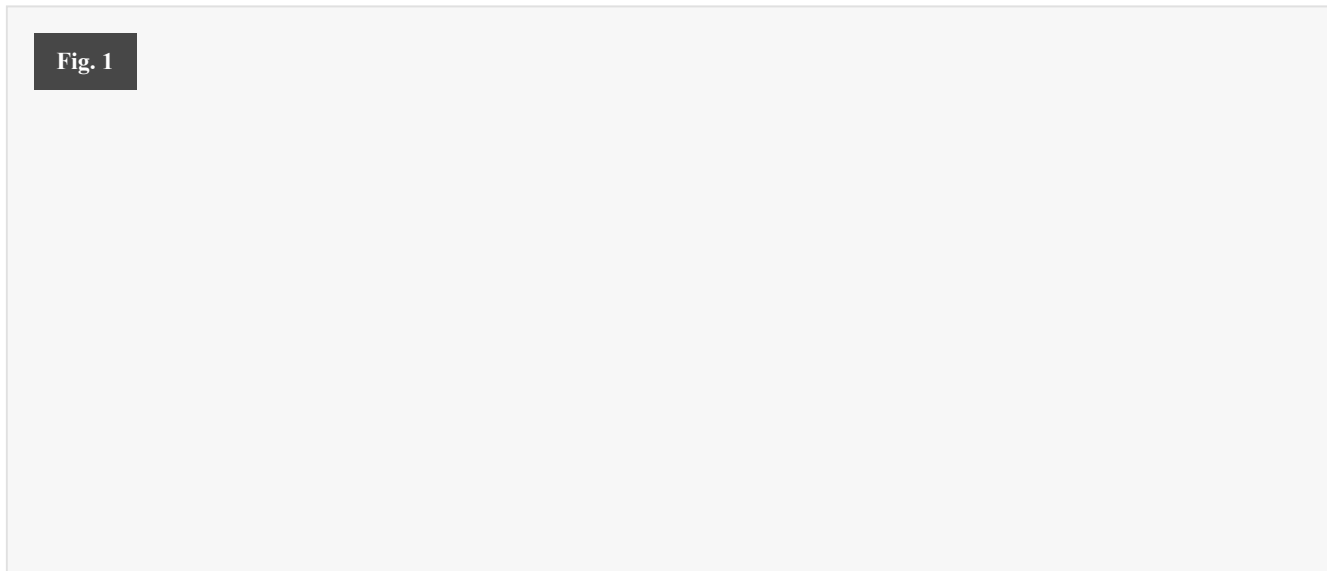
The remaining parts are classified as follows: in [Section 2](#), the GIDPC and the associated numerical model are explained. The digital twins and MOEO methods are included in [Section 3](#). Eventually, selection of diverse

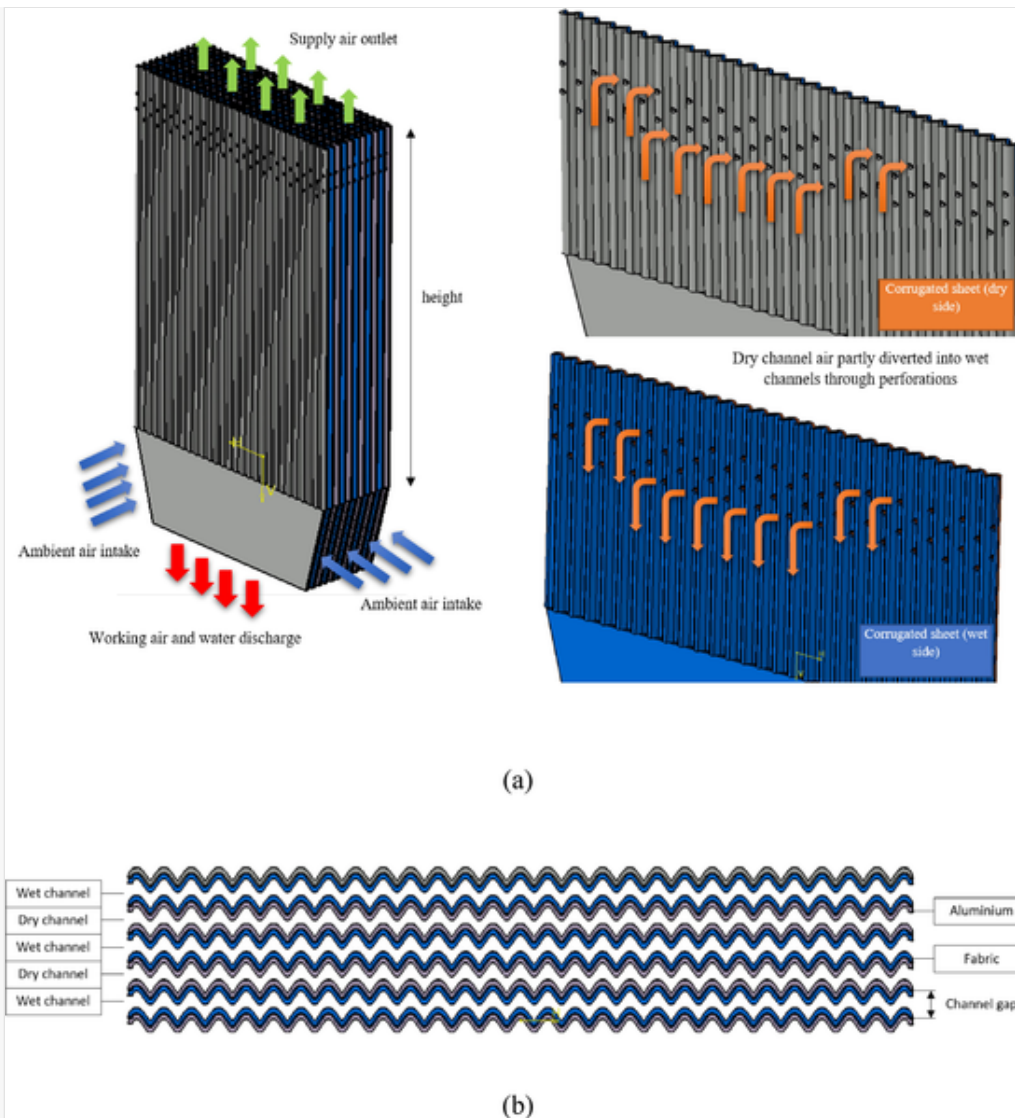
climate conditions, results and discussions are all provided in [Section 4](#).

2 System description (GIDPC)

In this section, a 4-kW counter-flow DPC with guideless irregular HMX (GIDPC) is explained. The GIDPC is constituted of a novel corrugated HMX, product and exhaust air fans, water supply/distribution system (which comprises a water distributor, a circulating water pump, a water tank). Among which, the HMX is the key innovative part of the GIDPC. The schematic drawing of the HMX of the GIDPC is shown in [Fig. 1](#). The proposed HMX is constructed by numerous layers which build the wet channels and dry channels for the cooling and evaporation processes. The wet channel is constructed by two facing wet surfaces while the dry channel is built by the adjacent two dry surfaces. On operation, the intake air enters the dry channel with specified temperature and humidity and while passing the dry channel, loses its heat to the adjacent wet channels by a remarkable decrease in its temperature. At the end of the dry channel the intake air is divided into two parts: working air and supply air. The working air, flows into the adjacent wet channel while the rest of it leaves the channel as the supply air. The amount of working air in the wet channel is specified by the working air fraction which receives considerable amount of heat transferred from the dry channel and the moisture from the surface of the wet channels. By completion of the heat and moisture transition, the working air leaves the wet channel as the warm and humidified air which is called exhaust air. Compared to the traditional flat plate HMX, the guideless irregular HMX has some remarkable advantages. For instance, removal of the supporting guides in the channels has led to an astronomical reduction in air flow resistance. Moreover, the heat transfer area has increased as a result of the corrugated surfaces. A super performance wet material layer used to cover the wet surfaces, i.e., Coolmax-fabric, has provided a higher water absorption capacity, higher diffusion area and more evaporation rate. As a result of such high absorption capacity, the intermittent water supply scheme has implemented in the water distribution system which can minimize the water usage and the water pump power consumption. It was shown that under the standard test condition [19], i.e. intake air dry bulb temperature of 37.8 °C and wet bulb temperature of 21.1 °C, the prototype of the GIDPC has achieved the wet-bulb efficiency of 114% and the dew point efficiency of 75%. In addition, a significant increase was achieved in COP value, i.e., 52.5, by the optimal working air ratio of 0.364, compared to the commercial DPC with the same dimensions (52.5 vs. 18).

Fig. 1





Heat and mass exchanger (a): heat and mass exchanger structure (b): corrugated surfaces (top view).

2.1 Numerical model

The finite element method is employed to treat the traditional mass and energy equations differentially, and the Newton iteration is applied to each considered element to pursue the equilibrium state in heat and mass transfer phenomena with some simplifying assumptions, i.e., heat transfer between the HMX and surrounding was ignored, heat and mass transfer was assumed to occur in steady state, the convective heat transfer in the walls of the channels were in vertical direction only, the walls were also considered to be impenetrable, thermal resistance of walls was ignored, and air within the channels was considered to be an incompressible gas. The numerical model was developed by applying the following equations to each of the selected computational elements along the channels [18]:

The air enthalpy difference between the inlet and outlet of the dry element is equal to the total heat transfer between the air flow in the dry element and channel walls as shown in Eq. (1).

Previous Version

$$\Delta i_{dry} = C_p \cdot Q_{m,dry} \cdot \Delta T_{dry} = h_{dry} \cdot (T_{dry} - T_w) \cdot \Delta A$$

Updated Version

$$\Delta i_{dry} = C_p \cdot Q_{m,dry} \cdot \Delta T_{dry} = h_{dry} \cdot (T_{dry} - T_w) \cdot \Delta A$$

(1)

Where C_p is specific heat capacity of air, $Q_{m,dry}$ is the mass flow rate of air in dry channel, T_{dry} is the air temperature in dry channel, T_w is the temperature of the wall and ΔA is the heat and mass transfer area of computational element. The difference of humidity ratio (HR) between the inlet and outlet of the wet element is equal to the amount of water evaporated across the wet surface as shown by **Eq. (2)**.

Previous Version

$$\Delta hum_{wet} = h_m \cdot \rho_{air,wet} \cdot (hum_w - hum_{air,wet}) \cdot \sigma \cdot \Delta A$$

Updated Version

$$\Delta hum_{wet} = h_m \cdot \rho_{air,wet} \cdot (hum_w - hum_{air,wet}) \cdot \sigma \cdot \Delta A$$

(2)

where h_m is the convective mass transfer coefficient between the working air flow and wet channel surface, $\rho_{air,wet}$ is density of the air in wet channel, hum_w and $hum_{air,wet}$ are the humidity ratio of the working air at the wet wall temperature and wet channel air temperature respectively and σ is the wettability of the surface material. The convective mass transfer coefficient between the working airflow and wet channel surface is expressed as a function of the convective heat transfer coefficient and the Lewis number ($h/h_m = \rho \cdot C_p \cdot Le^{1-n}$) where $n = 1/3$. The convective heat transfer coefficient between the airflow and the channel wall mainly depends on the flow regime (which is laminar in this study i.e., $52.31 < Re_{dry} < 1209$ and $5.38 < Re_{wet} < 1131$) and can be calculated using **Eq. (3)** as follows:

$$h = \frac{Nu \cdot \lambda}{De}$$

(3)

where Nu is the Nusselt number which depends on the air flow regime [18], λ and De (m) are the thermal conductivity and the equivalent diameter respectively.

The energy balance of air in the wet channel is considered by calculating the difference of air enthalpy between the inlet and outlet of a wet element through **Eq. (4)** which is equal to the sum of the heat transferred from the dry to wet elements and the change of airflow enthalpy in the wet element because of the evaporation.

Previous Version

$$\left\{ \begin{array}{l} \Delta i_{wet} = C_P \cdot Q_{m,wet} \cdot \varphi \cdot \Delta T_{wet} = \Delta Q_{wet} + \Delta i_{steam} \\ \Delta Q_{wet} = h_{wet} \cdot (T_w - T_{wet}) \cdot \Delta A \\ \Delta i_{steam} = h_m \cdot \rho_{air,wet} \cdot (hum_w - hum_{air,wet}) \cdot C_{P,steam} \cdot T_{wet,out} \cdot \sigma \cdot \Delta A \end{array} \right.$$

Updated Version

$$\left\{ \begin{array}{l} \Delta i_{wet} = C_P \cdot Q_{m,wet} \cdot \varphi \cdot \Delta T_{wet} = \Delta Q_{wet} + \Delta i_{steam} \\ \Delta Q_{wet} = h_{wet} \cdot (T_w - T_{wet}) \cdot \Delta A \\ \Delta i_{steam} = h_m \cdot \rho_{air,wet} \cdot (hum_w - hum_{air,wet}) \cdot C_{P,steam} \cdot T_{wet,out} \cdot \sigma \cdot \Delta A \end{array} \right.$$

(4)

where $Q_{m,wet}$ is mass flow rate in wet channel and φ is the working air fraction over the intake air.

As shown in **Eq. (5)**, the amount of water evaporated from the wet element surface is equal to variation of the water flow rate between the inlet and outlet of the computational wet element.

Previous Version

$$\Delta Q_{m,water} = h_m \cdot \rho_{air,wet} \cdot (hum_w - hum_{air,wet}) \cdot \sigma \cdot \Delta A$$

Updated Version

$$\Delta Q_{m,water} = h_m \cdot \rho_{air,wet} \cdot (hum_w - hum_{air,wet}) \cdot \sigma \cdot \Delta A$$

(5)

Water enthalpy difference between the inlet and outlet of a wet element is caused by heat transfer between the water and airflow in the dry/wet channels as well as the latent heat of the evaporated water as expressed in **Eq. (6)**.

Previous Version

$$\begin{cases} \Delta Q_{dry} = \Delta Q_{wet} + \Delta Q_{vap} + \Delta i_{water} \\ \Delta i_{water} = (Q_{m,water,out} \cdot T_{Wout} - Q_{m,water,in} \cdot T_{Win}) \cdot C_{P,water} \\ \Delta Q_{vap} = h_m \cdot \rho_{air,wet} \cdot (hum_w - hum_{air,wet}) \cdot en_{steam} \cdot \sigma \cdot \Delta A \\ en_{steam} = 2446 + 1.86T_{water} \end{cases}$$

Updated Version

$$\begin{cases} \Delta Q_{dry} = \Delta Q_{wet} + \Delta Q_{vap} + \Delta i_{water} \\ \Delta i_{water} = (Q_{m,water,out} \cdot T_{Wout} - Q_{m,water,in} \cdot T_{Win}) \cdot C_{P,water} \\ \Delta Q_{vap} = h_m \cdot \rho_{air,wet} \cdot (hum_w - hum_{air,wet}) \cdot en_{steam} \cdot \sigma \cdot \Delta A \\ en_{steam} = 2446 + 1.86T_{water} \end{cases}$$

(6)

where en_{steam} , is the latent heat of the evaporated water.

Generally, the IECs performance is evaluated by several common formula provided by ASHRAE [39] in which the cooling capacity and COP are the main performance parameters. The system performance can also be evaluated using other metrics such as wet-bulb efficiency and dew point efficiency. The cooling capacity can be expressed by **Eq. (7)** as follows:

$$Q_{cooling} = C_p (T_{dry,in} - T_{dry,out}) (1 - \varphi) Q_{m,dr,in}$$

(7)

where $Q_{cooling}$ is cooling capacity, C_p is the specific heat capacity, $T_{dry,in}$ is the intake air temperature in dry channel, $T_{dry,out}$ is the outlet air temperature in the dry channel, φ is working air fraction, and $Q_{m,dr,in}$ is mass flow rate of intake air in dry channel.

COP can be expressed as **Eq. (8)** as follows:

$$COP = \frac{Q_{cooling}}{W_{fan} + W_{pump}}$$

(8)

where, W_{fan} and W_{pump} are the electrical power consumed by the fan and the pump respectively.

Wet-bulb efficiency evaluates the system capability in reducing the intake air temperature to its wet-bulb temperature. Similarly, the dew point efficiency considers the system potential in reducing the intake air temperature to its dew point temperature as shown in **Eq. (9)**:

$$\begin{cases} \varepsilon_{wb} = \frac{T_{dry,in} - T_{dry,out}}{T_{dry,in} - T_{dry,in,wb}} \\ \varepsilon_{dp} = \frac{T_{dry,in} - T_{dry,out}}{T_{dry,in} - T_{dry,in,dp}} \end{cases} \quad (9)$$

where, ε_{wb} is the wet bulb efficiency and $T_{dry,in,wb}$ is the wet-bulb temperature of the intake air in dry channel, ε_{dp} is the dew point efficiency and $T_{dry,in,dp}$ is the dew point temperature of the intake air in dry channel.

$$\Delta P = \left(\xi + \lambda_f \frac{1}{D_h} \right) \frac{\rho U^2}{2} \quad (10)$$

where ΔP is pressure drop, ξ is coefficient of local resistance, λ_f is coefficient of friction resistance, D_h is hydraulic diameter, ρ is density and U is the air velocity.

Surface area of the layers is a parameter that is considered to control the cost which can be calculated using the Eq. (11) as follows:

Previous Version	$A_s = (N_L)(H)(w)$
Updated Version	$A_s = N_L \cdot H \cdot w$

(11)

where A_s is the surface area, N_L is the number of layers, H is height of the HMX and w represents the width of the surface. In the current GIDPC, the width of the corrugated surface is supposed to have the value of 0.39 (m) [19].

3 Proposed methods: digital twins and multi objective evolutionary optimization

This section has two main contribution; I) The digital twins using FFNN is developed to follow the system behaviour; II) The MOEO using GA is applied to obtain the optimal operating and design parameters of the system in diverse climates.

3.1 Digital twins using Feed-Forward Neural network

Digital Twins can be defined as a digital replication of a physical entity. It can be also combined with the Internet of Things (IoT) and/or augmented reality. However, in the simplest case, it would be just a system identification for different purposes such as abnormality detection and system optimization [40]. Black box, grey box and weight box models are three classes of the system identification known as the main part of digital twins. The FFNN is used as a black box and data-driven model to build the digital twins. Neural Networks (NNs) are machine learning algorithms which can be used for data-driven prediction, regression and classification. NNs are inspired from human brain and are multi-layer networks of neurons which are constructed by: an input layer which accepts the input variables, single or numerous hidden layers, and an output layer which accepts the output variables.

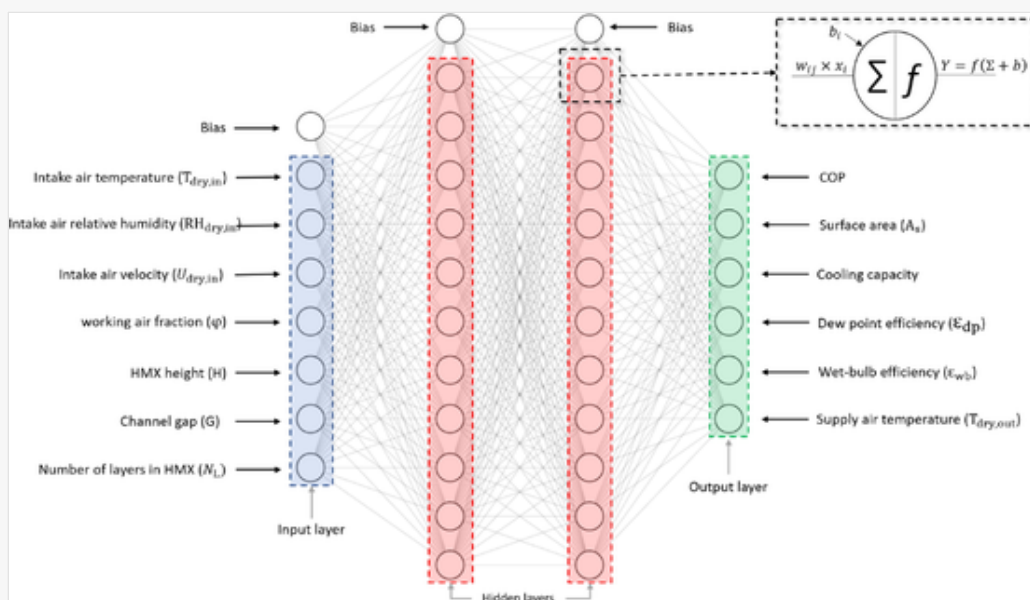
The architecture of a FFNN, which is a specific type of NN is depicted in Fig. 2 where each neuron within each layer is connected to every one of the neurons in the following layer. Initialization process triggers when each of the connections is weighted by a random value which will be updated during the training procedure to reach the best fit with the lowest possible error values. In addition, there is a bias parameter which is used to adjust the output values of the weighted sum of the inputs to the neuron. Bias is a random constant which helps the model in a way that it can fit best for the given data.

$$x_j = \sum_{i=1}^{i=n} w_i x_i + b_i$$

(12)

where w_i represents the weight connecting the neuron x_i to neuron x_j in the next layer, n represents the number of the connections, and b_i is the corresponding bias.

Fig. 2



Structure of the FFNN.

Activation functions are needed to attach to each neuron and their role is to determine the importance of each neuron's input in prediction of the outputs and to normalize the output of the neurons. Different activation functions are compared and it is found that the performance of the network in terms of Mean Square Error (MSE) is the best when the activation function is hyperbolic tangent sigmoid for the current GIDPC big dataset which performs through the function below:

$$y_j = f(x_j) = \frac{e^{x_j} - e^{-x_j}}{e^{x_j} + e^{-x_j}} \quad (13)$$

where y_j is the activated value of the neuron j .

Randomly selected weights and biases are iteratively optimized through back-propagation process until the considered evaluation metric, e.g., the mean square error, is minimised. The back-propagation is an essence step in minimising the errors and maximising the model generalization [41]. The holdout cross-validation is used to divide the big dataset into three sources: a training data set (70%), a validation data set (15%), and a testing data set (15%). The training data set is used to estimate the network weights, while the validation data set is used to monitor the network and calculate the minimum error during the iterations till network is stopped. The test data set is unseen data by network and task of the test data set is to decrease the bias and generate unbiased estimates for predicting future outcomes and generalizability. The test data set is used at the end of the iteration process for evaluating the performance of the model from an independently drawn sample.

A Bayesian Regularization (BR) is used as a regularization method in optimizing the weight and bias values, which is the linear combination of Bayesian methods and NN to determine the optimal regularization parameters. BR technique implements certain prior distributions on the model parameters as follows [42]:

$$F = \beta E_D(D|w, M) + \alpha E_w(w|M); \quad D = \{X, Y\} \quad (14)$$

where D represents the big data set, i.e., X represents the inputs and Y represents the outputs, $E_D(D|w, M)$ is the sum of squared estimation errors, M represents the network structure, β and α are estimated hyper-parameters. $E_w(w|M)$ is sum of the weights' squares which intends to decrease the overfitting probability of the model [43]. Density function is used for updating the weights according to Bayes' rule. The posterior distribution of w given α , β , D , and M can be written as:


$$P(w|D, \alpha, \beta, M) = \frac{P(D|w, \beta, M) P(w|\alpha, M)}{P(D|\alpha, \beta, M)} \quad (15)$$

where $P(D|w, \beta, M)$ is likelihood function of w , $P(w|\alpha, M)$ is the prior distribution of weights under M , which is the probability of observing the data given w and $P(D|\alpha, \beta, M)$ is a normalization factor or evidence for

hyperparameters α and β .

In this study, as listed in Table 1, main operating and design parameters i.e., temperature, relative humidity and velocity of the intake air, working air fraction, HMX height and channel gap, and number of layers in HMX structure are all considered as input parameters. Additionally, main performance parameters i.e., supply air temperature, cooling capacity, COP, dew point efficiency, wet-bulb efficiency and surface area of the layers are considered as output parameters. The big data set is created using the newly defined operating ranges based on the literature [32,37] and with a purpose of covering wider ranges, by the validated numerical model [18].

Table 1

 The table layout displayed in this section is not how it will appear in the final version. The representation below is solely purposed for providing corrections to the table. To preview the actual presentation of the table, please view the Proof.

Big Dataset specifications.

Type of parameters	input parameters	Minimum	Maximum
Operating parameters	$T_{\text{dry,in}}$ (°C)	25	45
	$RH_{\text{dry,in}}$ (-)	0.10	0.80
	$U_{\text{dry,in}}$ (m/s)	0.30	3.30
	φ (-)	0.10	0.90
Design parameters	H (m)	0.80	3.00
	G (m)	0.004	0.008
	N_L (-)	100	200
Number of data points	Dataset breakdown		
	Training	Validation	Testing
78,125	70%	15%	15%

3.2 Multi objective evolutionary optimization using genetic algorithm

Generally, optimization techniques are classified into four main categories [44]: constrained, multimodal, multi objective and combinatorial. It can also be categorised into classical and metaheuristic optimization [45]. In this study, the constrained multi-objective evolutionary optimization (MOEO) using Genetic Algorithm (GA) known as one of the random-based Evolutionary Algorithms (EAs) is selected as an optimization tool. Optimization which will help to reach the maximum potential of the GIDPC by identifying the optimum values of operating and design parameters and it can deal with system nonlinearity and ignores the local

minimums of the problem. Optimization is done in MATLAB and its correctness was validated in different studies [46,47]. The convergence of the MOEO is investigated through the cost versus number of iterations.

The cooling capacity, COP, wet-bulb efficiency and surface area of the layers are selected as objectives as they inherently consider the economic and engineering characteristics of the system simultaneously. The reason for selecting the cooling capacity and COP is to maximise the cooling performance and minimise the power consumption of the system simultaneously. Although the cooling capacity is included in the COP calculations but considering the COP only, will lead to irrational results as the focus may be only on reducing the power consumption only. Moreover, maximising the wet-bulb efficiency minimises the supply air temperature of the GIDPC. Eventually, minimising the surface area of the layers will lead to lower production cost. Considering a single objective can result in irrational solutions by ignoring crucial trade-offs in identifying the optimum values. For instance, the cooling capacity of a DPC can be improved by increasing the length of the channels whereas longer channels can lead to lower COP and higher pressure drop (more fan power) [48]. Thus, a multi objective optimization is necessary to find the best optimum balance between the objectives.

The optimization function is defined by fitness function and the constraint function. The trained FFNN, is the fitness function to be optimized which sets the variables of the problem and the optimization objectives. The constraint function implements the parameters defined ranges as restrictions on the fitness function.

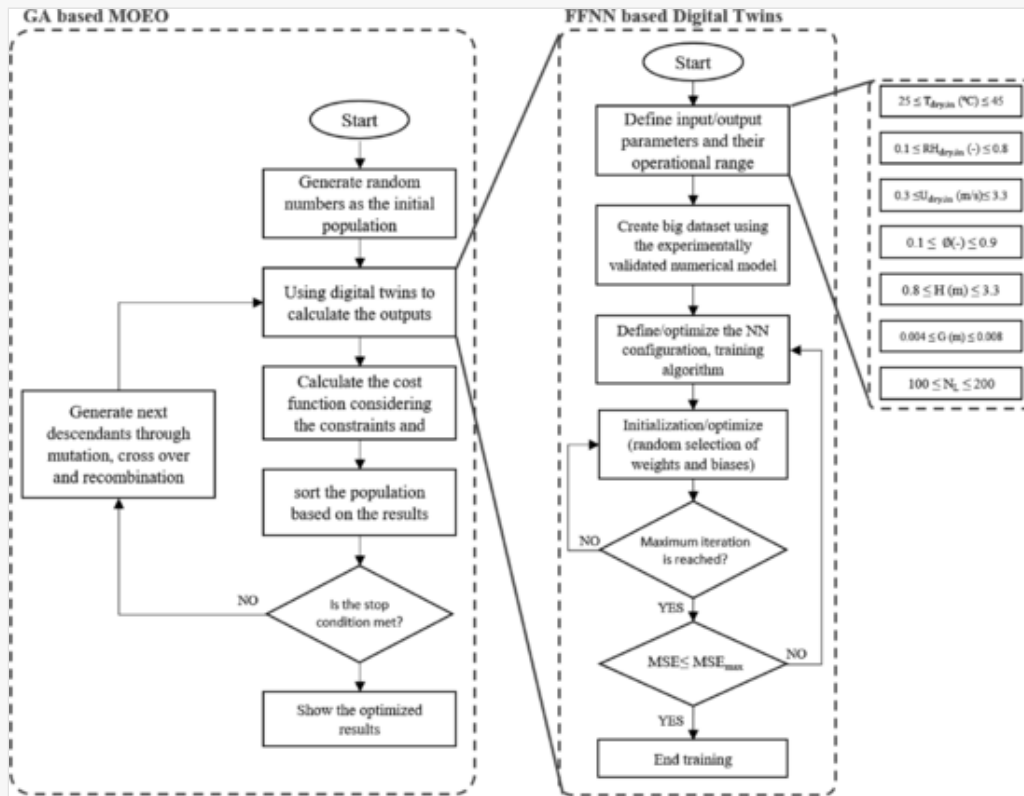
In the present optimization method, the input parameters are assumed as genotype and output parameters are considered as phenotype. Out of seven input parameters listed in Table 1, the temperature and relative humidity of the intake air vary by climates but the remaining five input parameters are chosen as decision variables. Hence, for each specific climate, a MOEO is performed, which will result a unique optimum design for that climate.

In each generation, selection functions pick the most valuable genes which are chosen as the parents of the next generation and then the multi point crossing over procedure is performed on them. Among these, the random genes are added to the population as mutation functions and this procedure is repeated until ultimate criteria are established. Different conditions can be set to stop this process which was reaching the maximum iterations of 200 in this study. The flowchart of the optimization process is shown in Fig. 3. In addition, configured settings and parameters for the proposed optimization are summarized in Table 2. The trial-and-error is the most common way to select the listed parameters. However, the plot of cost versus iterations, system's nonlinearity, number of inputs were the main factors in selecting these parameters. The cost function in this study is considered as follows:

$$J(T_{dry,in}, RH_{dry,in}, U_{dry,in}, \varphi, H, G, N_L) = W_1 \frac{Q_{cooling}}{RQ_{cooling}} + W_2 \frac{COP}{RCOP} + W_3 \frac{\varepsilon_{wb}}{R\varepsilon_{wb}} + W_4 \frac{RA_s}{A_s} \quad (16)$$

where $T_{dry,in}$ and $RH_{dry,in}$ are predefined based on the climates, W is the weights for each objective, $RQ_{cooling}$, $RCOP$, $R\varepsilon_{wb}$, and RA_s are used to normalize the output values or objectives.

Fig. 3



Detailed illustration of the methods discussed in section 3.

Table 2

i The table layout displayed in this section is not how it will appear in the final version. The representation below is solely purposed for providing corrections to the table. To preview the actual presentation of the table, please view the Proof.

Genetic Algorithm settings.

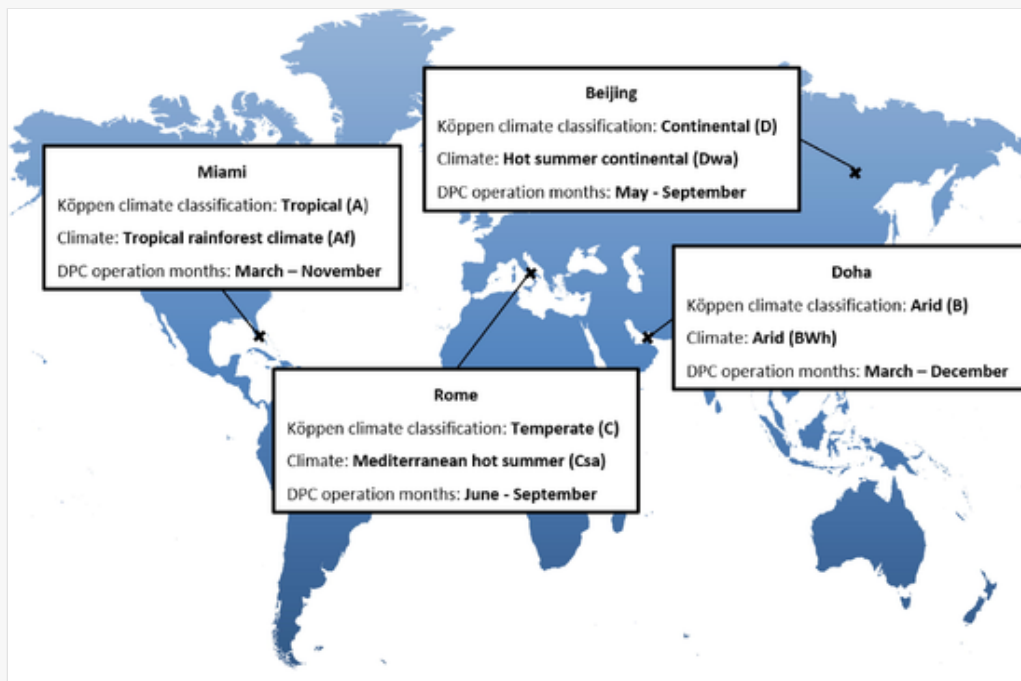
Type of parameter	Rate or type of consideration
Population Size	40
Iteration or Decades	200
Percentage of Mutations	35%
Type of Mutations	Random Number Generation
Percentage of Crossover	50%
Type of Crossover	2 Point Crossing Over
Percentage of Recombination	15%

4 Results and discussions

4.1 Selected climates

According to the Köppen–Geiger's climate classification [38] and considering the defined ranges, out of seven existed climates, warm periods of four different climates i.e., Tropical rainforest climate, Arid, Mediterranean hot summer and Hot summer continental are identified as suitable regions for the DPC operation. One representative city for each climate is selected and, in each city, the warm months for the DPC operation are identified. The criteria for selection of the operating months is the common defined ranges of the temperature and relative humidity of the intake air (see Table 1). The four suitable classifications and their representative climates and cities as well as the operating months are all shown in Fig. 4. In addition, the monthly temperature and relative humidity of the representative cities [49] and the corresponding average values of the operating months are summarized in Table 3.

Fig. 4



Selected climates and their representative cities.

Table 3

i The table layout displayed in this section is not how it will appear in the final version. The representation below is solely purposed for providing corrections to the table. To preview the actual presentation of the table, please

view the Proof.

Monthly and average weather data of each city [49].

Month	Miami		Doha		Rome		Beijing	
	T(°C)	RH(-)	T(°C)	RH(-)	T(°C)	RH(-)	T(°C)	RH(-)
January	24	0.74	22	0.72	12	0.76	2.50	0.44
February	24	0.73	23	0.70	13	0.76	5	0.44
March	26	0.70	27	0.62	15	0.75	12	0.44
April	28	0.69	33	0.52	18	0.75	20	0.45
May	29	0.71	39	0.43	22.90	0.75	26	0.53
June	30	0.72	42	0.41	26	0.74	30	0.60
July	31	0.72	42	0.50	27.90	0.73	31	0.75
August	30.50	0.72	40.50	0.54	28.10	0.75	30	0.78
September	30.40	0.75	39.50	0.62	27	0.75	27	0.69
October	28.50	0.76	36	0.63	22.90	0.76	19.90	0.60
November	26	0.72	29.90	0.66	17	0.79	20	0.58
December	23.90	0.74	25	0.71	12	0.79	5	0.50
Average in operating months	28.82	0.72	35.39	0.56	27.25	0.74	28.80	0.67

4.2 Feed-forward neural network configuration

NN is mainly configured by two main hyperparameters that defines the structure the network, i.e., the number of layers and the number of neurons in each hidden layer. The most common method to spot the preminent values of these hyperparameters for a specific problem is via calibration by a robust test harness. Therefore, several models with different hyperparameters are constructed until the desired accurate model identified. The model reconstruction stopped when no significant improvement in accuracy metrics i.e., MSE and coefficient of determination (R^2) is seen:

$$\text{MSE} = \frac{\sum_{i=0}^N (\hat{Y}_i - Y_i)^2}{N}$$

(17)

$$R^2 = 1 - \frac{\sum_{i=0}^N (\hat{Y}_i - Y_i)^2}{\sum_{i=0}^N (\bar{Y}_i - Y_i)^2} \quad (18)$$

where, Y represents the real value of the considered output, \hat{Y} represents its predicted value by FNNN and N represents the number of operating conditions.

As listed in Table 4, ten different configurations are compared in terms of MSE and R^2 values.

Table 4

i The table layout displayed in this section is not how it will appear in the final version. The representation below is solely purposed for providing corrections to the table. To preview the actual presentation of the table, please view the Proof.

Comparison of different NN models.

Model	Number of layers	Neurons No in 1st layer	Neurons No in 2nd layer	MSE	R2
1	1	10	NA	1483.89	0.98
2	1	20	NA	182.21	0.99
3	1	30	NA	112.33	0.99
4	2	30	10	12.86	1
5	2	30	20	6.74	1
6	2	40	30	2.39	1
7	2	40	40	1.19	1
8	2	45	40	0.9	1
9*	2	45	45	0.04	1
10	2	50	45	0.03	1

Due to the relatively high number of operating conditions in the big dataset, i.e., 78125, firstly, the FFNN model with a single hidden layer and 10 neurons is configured. The MSE value has revealed that more robust configuration is needed in order to reduce the MSE and increase the accuracy of the network. Thus, the network complexity is increased gradually by increasing the number of hidden layers and neurons till no significant improvement observed in the MSE value. Model number 9 with 2 hidden layers, and 45 neurons in each hidden layer is selected as the final network since it is accurate enough with MSE value of 0.04 to stop the robust test harness. However, one more model with a slight improvement, i.e., model number 10, is

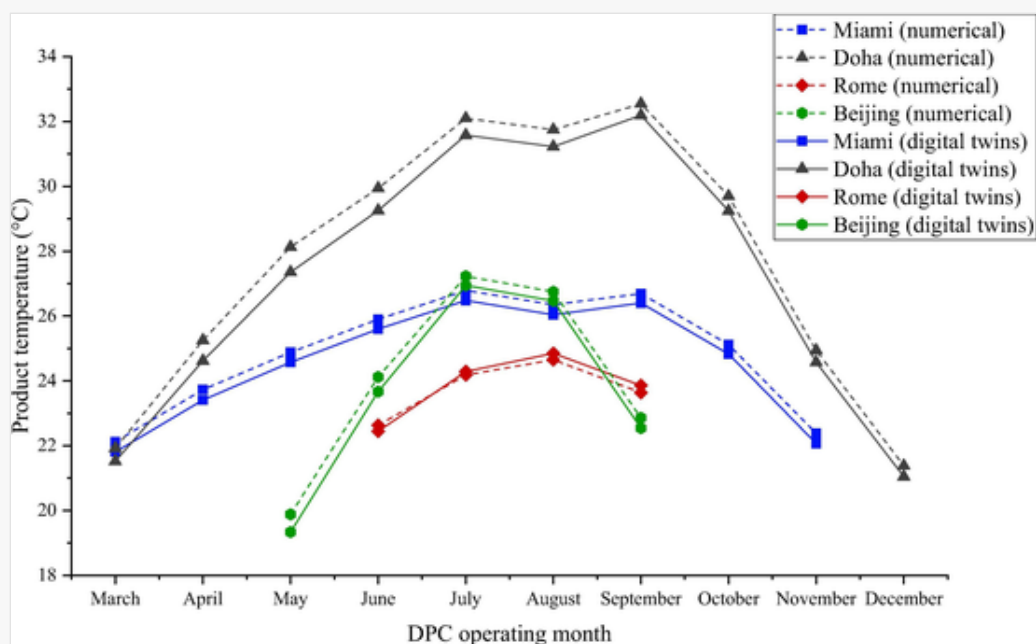
constructed to compare it with the selected model. It can be seen that, although the model was improved, i.e., with MSE of 0.03, but no significant accuracy added to the network. Hence, the model No. 9 is selected for the performance prediction of the GIDPC and GA optimization.

4.3 FFNN model validation: comparison of the supply air temperature

The developed NN model is validated by the numerical model which was validated experimentally by a 4-kW GIDPC. Although the FFNN model is inherently validated by being trained and validated through the big dataset which was constructed by the numerical model but to illustrate this validation, the predicted temperature of the supply air is compared between the FFNN and numerical models. The idea of selecting the temperature of the supply air, as the comparison parameter for the validation, is based on the key role of this factor in system performance evaluation. Supply air temperature is directly considered in performance parameters calculations, e.g., cooling capacity, and its value is influenced by other key parameters such as intake air parameters, working air fraction and HMX dimensions [39].

Therefore, the supply air temperature predicted by the models are compared in each climate and the results are shown in Fig. 5. The comparison is done over the identified operating months by holding the key parameters unchanged, i.e., the air velocity, air working fraction, HMX height, channel gap and number of layers were kept at 3 (m/s), 0.44, 1 (m), 0.005 (m) and 160 respectively which are also defined as the base system parameters. The results revealed that the predictions made by two models are in good agreement in which the maximum discrepancies between the numerical and FFNN models in Miami, Doha, Rome and Beijing are recorded as 0.32 °C, 0.77 °C, 0.21 °C and 0.54 °C respectively.

Fig. 5



Comparison of the supply air temperature of the base system by numerical and digital twins models in operating months.

4.4 Optimization results

Average climate data, which were listed in Table 3, are taken to operate the MOEO in order to identify the optimum decision variables in each city. The reason for taking the average data instead of monthly data is because a single GIDPC unit with optimum operating and design parameters will be introduced for each representative city. The MOEO is operated for different weight values, which have the total value of one, in order to choose the best possible cost function. In this study, the priority is to choose the best approach in which the majority of the objectives can hold better values than the base system. Therefore, the results, as listed in Tables 5–8, revealed that out of five considered weight distributions (i.e., equal weights for each objective, and dominant weights for each of the four considered objectives), the equally distributed weights (i.e., 0.25) are the most desired condition for optimising the GIDPC performance in which the COP and surface area values are significantly improved and the cooling capacity and wet bulb efficiency are almost same as the base system. But, considering the cooling capacity as the dominant objective ($W1 = 0.85$), results in significantly lower COP and higher surface area values. Considering the COP as the dominant objective ($W2 = 0.85$), has caused in low cooling capacity and wet bulb efficiency. Taking the wet bulb efficiency as the dominant objective ($W3 = 0.85$), has led to significantly low COP and cooling capacity values. Although considering the surface area as the dominant weight ($W4 = 0.85$) gives desired values for COP and efficiency but compared to the equal weights, the cooling capacity is substantially lower. Consequently, the equally distributed weights are chosen as the best solution for optimising the system performance. However, the cooling capacity and efficiency values are sacrificed due to the improved COP and surface area values.

Table 5

i The table layout displayed in this section is not how it will appear in the final version. The representation below is solely purposed for providing corrections to the table. To preview the actual presentation of the table, please view the Proof.

Identified optimum parameters in Miami.

City	Design Weights				Decision variables					Objectives			
	W1	W2	W3	W4	$U_{dry,in}$ (m/s)	φ (-)	H (m)	G (m)	N_L (-)	$Q_{cooling}$	COP	ϵ_{wb}	A_s
Miami	0.25*	0.25*	0.25*	0.25*	2.00	0.21	0.80	0.006	159.82	1046.60	30.42	0.83	50.57
	0.85	0.05	0.05	0.05	2.93	0.23	2.78	0.007	159.97	2176.29	10.68	0.89	126.86
	0.05	0.85	0.05	0.05	2.00	0.16	0.81	0.007	100.28	744.27	35.36	0.69	31.81
	0.05	0.05	0.85	0.05	2.00	0.28	1.27	0.004	100.09	670.28	16.48	1.47	50.04
	0.05	0.05	0.05	0.85	2.00	0.21	0.82	0.006	100.15	721.09	32.23	0.86	31.87
	Base system				3.00	0.44	1.00	0.005	160.00	1112.92	9.39	1.01	62.49

Table 6

i The table layout displayed in this section is not how it will appear in the final version. The representation below is solely purposed for providing corrections to the table. To preview the actual presentation of the table, please view the Proof.

Identified optimum parameters in Doha.

City	Design Weights				Decision variables					Objectives			
	W1	W2	W3	W4	$U_{dry,in}$ (m/s)	ϕ (-)	H (m)	G (m)	N_L (-)	$Q_{cooling}$	COP	ϵ_{wb}	A_s
Doha	0.25*	0.25*	0.25*	0.25*	2.00	0.25	0.81	0.005	159.92	1972.96	51.88	0.99	51.13
	0.85	0.05	0.05	0.05	2.75	0.22	2.25	0.007	159.95	3711.33	25.20	0.85	143.01
	0.05	0.85	0.05	0.05	2.00	0.16	0.80	0.007	105.28	1437.84	64.73	0.67	32.33
	0.05	0.05	0.85	0.05	2.01	0.28	1.43	0.004	100.27	1206.68	26.26	1.38	57.23
	0.05	0.05	0.05	0.85	2.00	0.204	0.83	0.005	100.21	1267.19	53.08	0.94	31.94
	Base system				3.00	0.44	1.00	0.005	160.00	2205.4	18.58	1.01	62.50


Table 7

i The table layout displayed in this section is not how it will appear in the final version. The representation below is solely purposed for providing corrections to the table. To preview the actual presentation of the table, please view the Proof.

Identified optimum parameters in Rome.

City	Design Weights				Decision variables					Objectives			
	W1	W2	W3	W4	$U_{dry,in}$ (m/s)	ϕ (-)	H (m)	G (m)	N_L (-)	$Q_{cooling}$	COP	ϵ_{wb}	A_s
Rome	0.25*	0.25*	0.25*	0.25*	2.00	0.21	0.82	0.006	159.82	928.37	26.58	0.84	51.65
	0.85	0.05	0.05	0.05	2.70	0.24	2.66	0.007	159.84	1804.46	10.88	0.91	169.82
	0.05	0.85	0.05	0.05	2.00	0.17	0.80	0.007	100.04	656.83	31.30	0.70	31.77
	0.05	0.05	0.85	0.05	2.00	0.28	1.24	0.004	100.11	599.08	15.17	1.43	48.64
	0.05	0.05	0.05	0.85	2.00	0.20	0.80	0.006	101.74	644.07	29.12	0.84	31.89
	Base system				3.00	0.44	1.00	0.005	160.00	836.63	7.24	1.00	62.50

Table 8

 The table layout displayed in this section is not how it will appear in the final version. The representation below is solely purposed for providing corrections to the table. To preview the actual presentation of the table, please view the Proof.

Identified optimum parameters in Beijing.

City	Design Weights				Decision variables					Objectives			
	W1	W2	W3	W4	$U_{dry,in}$ (m/s)	ϕ (-)	H (m)	G (m)	N_L (-)	$Q_{cooling}$	COP	ϵ_{wb}	A_s
Beijing	0.25*	0.25*	0.25*	0.25*	2.00	0.23	0.84	0.006	159.85	1234.23	34.20	0.85	52.76
	0.85	0.05	0.05	0.05	2.72	0.24	2.54	0.007	159.93	2375.10	14.66	0.89	161.32
	0.05	0.85	0.05	0.05	2.00	0.17	0.80	0.007	100.5	858.34	40.52	0.67	31.80
	0.05	0.05	0.85	0.05	2.00	0.30	1.36	0.004	100.13	771.09	17.52	1.42	54.24
	0.05	0.05	0.05	0.85	2.00	0.22	0.80	0.005	102.32	827.28	36.35	0.86	31.92
	Base system				3.00	0.44	1.00	0.005	160.00	1372.83	11.80	0.98	62.51

4.4.1 Optimum intake air velocity

The intake air velocity is a factor which has a remarkable impact on system performance as it directly effects the cooling capacity, and rate of heat and mass transfer within the HMX. A higher velocity is associated with larger pressure drop which results in more power consumption and consequently less COP values which are not desirable in optimization and performance evaluation of DPCs. Thus, calibrating the air velocity is challenging, as investigated by Xu et al. [18], and a robust trade-off considering the effect of several parameters was required to identify the optimum value in each climate. The GA algorithms revealed that the optimum air velocity is almost 2 (m/s) in all climates which is lower than the velocity in the base system which was 3 (m/s). Tendency of the GA to give a lower value for the air velocity was somehow expected as the higher COP values are aimed. Hence, it can be concluded that a trade-off by GA has concluded that the lower range of the intake air velocity is weighted more than the maximum allowable value of 3.3 (m/s).

4.4.2 Optimum working air ratio

The working air ratio is defined as the ratio of the exhaust air to the total intake air. Higher working air ratio will lead to less supply air flow and consequently more temperature drop will occur in intake air which flows inside the HMX dry channels. As a result, at a very high working air ratio, the dew point efficiency will increase but it will lead to lower COP and cooling capacity values. In addition, the low supply air flow will remain as an unfavourable issue. Thus, similar to the air velocity, calibrating the working air ratio is another important challenge in DPC operation which requires a trade-off between the other involved parameters in

different climates. The working air fraction in the base system is taken as 0.44 which was based on the experimental study of the M30 (Coolerado USA) DPC [10]. GA algorithm revealed that the optimum working air ratio is ranging from 0.21 to 0.25 which are less than 0.44 in operating condition of the base system. It means that less working air and more supply air compared to the base system operation condition leads to better system performance. The optimum working air ratio holds almost the same value of 0.21 in Miami and Rome where it is 0.25 in Doha and 0.23 in Beijing.

4.4.3 Optimum HMX height

Higher HMX height normally results in better DPC performance [18] in terms of cooling capacity by providing more heat transfer area in the HMX sheets but on the contrary it leads to higher pressure drop along the heat exchanger, higher fan power, larger surface area and higher construction costs simultaneously [50]. Therefore, GA needed a trade-off to recognize the optimum height values. The identified optimum HMX height is identified to be in the range of 0.80–0.84 (m) which are lower than the base value of 1 m. It is identified that the DPC had the best performance with the minimum height value of 0.80 (m) in Miami and by the maximum height of 0.84 (m) in Beijing. The optimum HMX height in Doha and Rome were detected as 0.81 (m) and 0.82 (m) respectively. As a result, it can be seen that the optimum values are less than the maximum constraint which was 3 (m), less than the base system value which was 1 (m), and tend to hold a lower band value of the range.

4.4.4 Optimum channel gap and number of layers

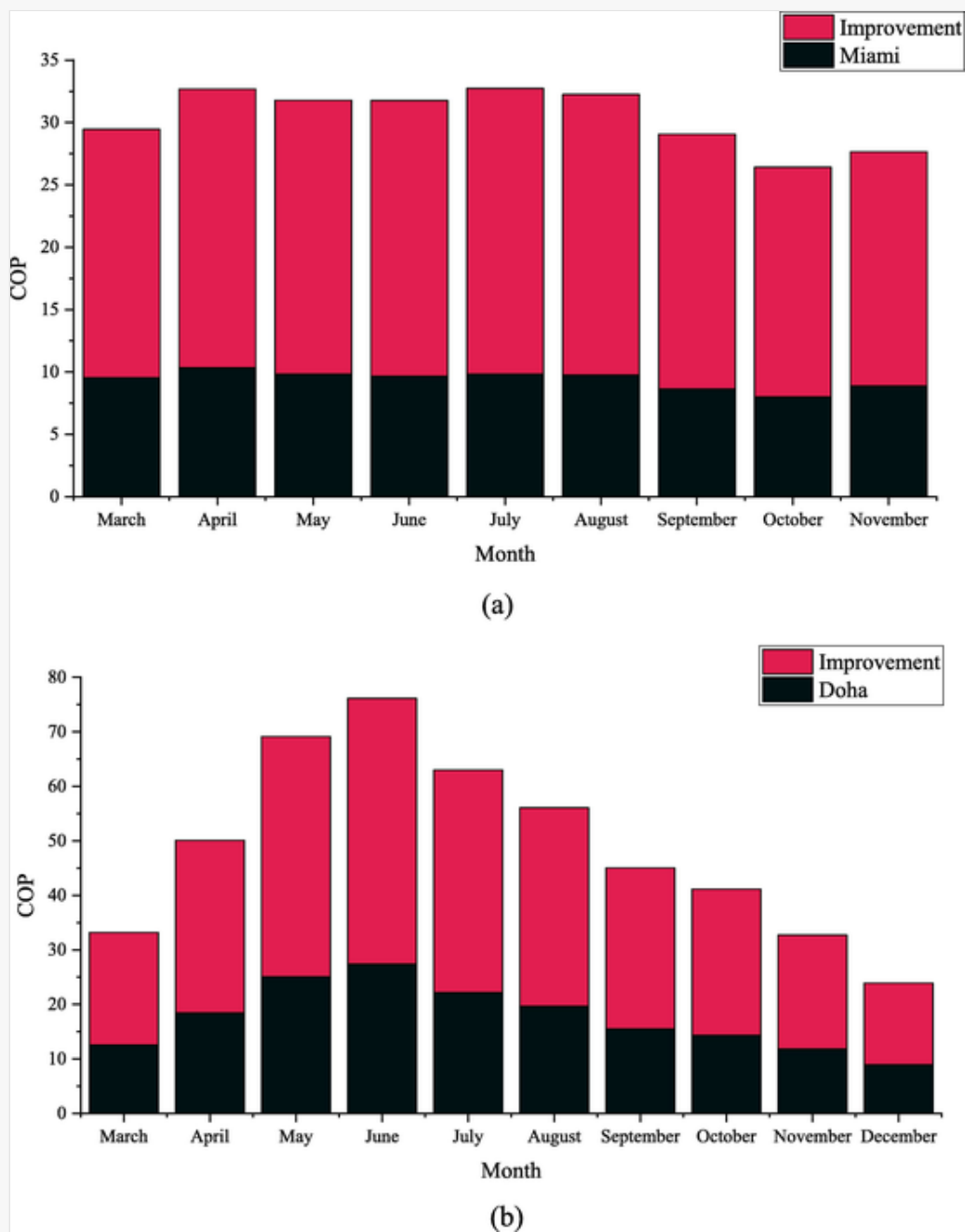
The smaller channel gap will cause higher pressure drop and consequently will result in higher fan power and lower COP values. To the contrary, the larger channel gap will lead to higher mass flow rate and higher cooling capacity. Similarly, more layers can be considered as an important factor in increasing the pressure drop, surface area and construction cost. In addition, an increase of these parameters will lead to more evaporation area and more heat transfer from dry channel to wet channel. Therefore, like previous decision variables, a careful trade-off is needed to identify the optimum values in each climate. GA algorithm revealed that the optimum values are higher than the base system with channel gap of 0.005 (m) and number of layers of 160. The optimum value of channel gap is in the narrow range of 0.005–0.006 (m). Similarly, optimum values of the number of layers are almost same in all cities i.e., 159–160. The channel gap multiplied by the number of layers gives the width of the HMX that was 0.8 (m) in the base system but it varies in the range of 0.79–0.95 (m) in the optimum conditions. Hence, it is concluded that similar to the height of the system, the lower values of channel gap and number of layers are desired as they lead to a substantial decrease in surface area of the layers.

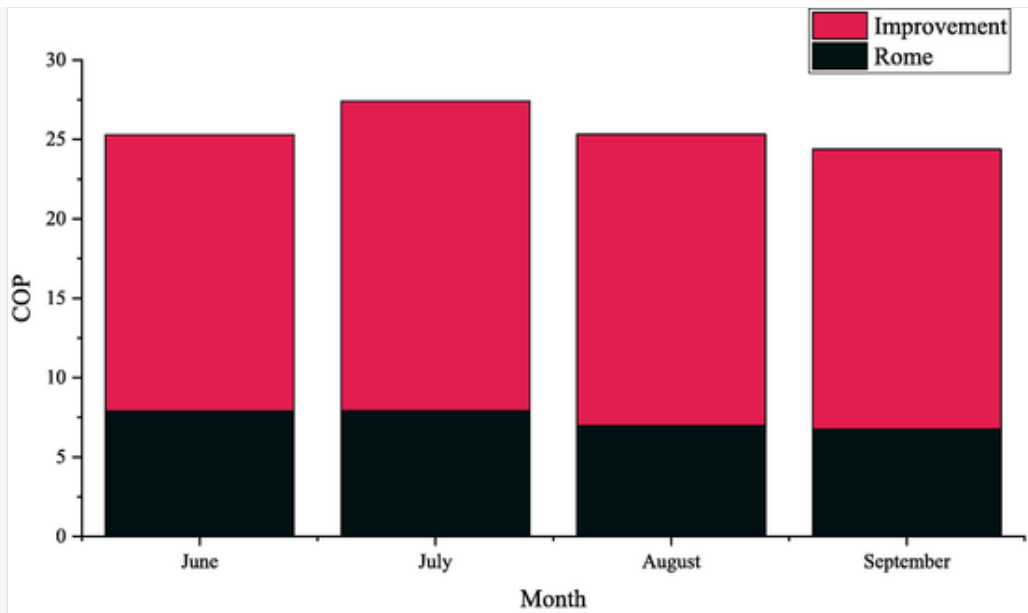
4.5 System operation in optimum conditions

The identified optimum operating and design parameters revealed that remarkable improvements have occurred in COP and surface area values but other performance parameters i.e., cooling capacity, dew point and wet-bulb efficiencies, and supply air temperature are almost remained unchanged as all shown in Figs. 6–11. The main reason for this behaviour lies in the fact that the changes in the main operating and design parameters i.e., reduction in working air fraction and air velocity and height of the HMX have sacrificed the

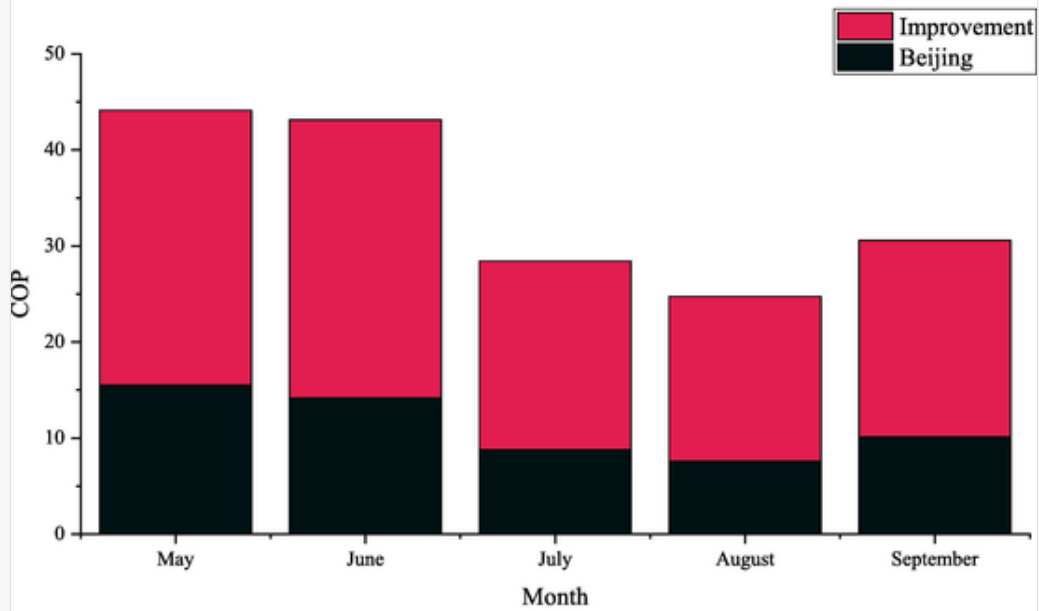
unchanged performance parameters. However, they have caused a remarkable improvement in COP and surface area which will lead to significant reduction in power consumption and production cost. Detailed discussion on the system behaviour is firstly presented by studying the monthly performance of the system under identified optimum conditions in each region, and secondly, the optimization effect on annual performance of the system is investigated.

Fig. 6





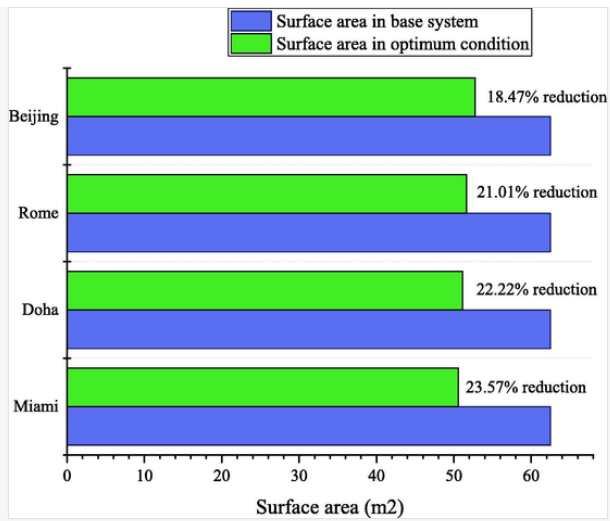
(c)



(d)

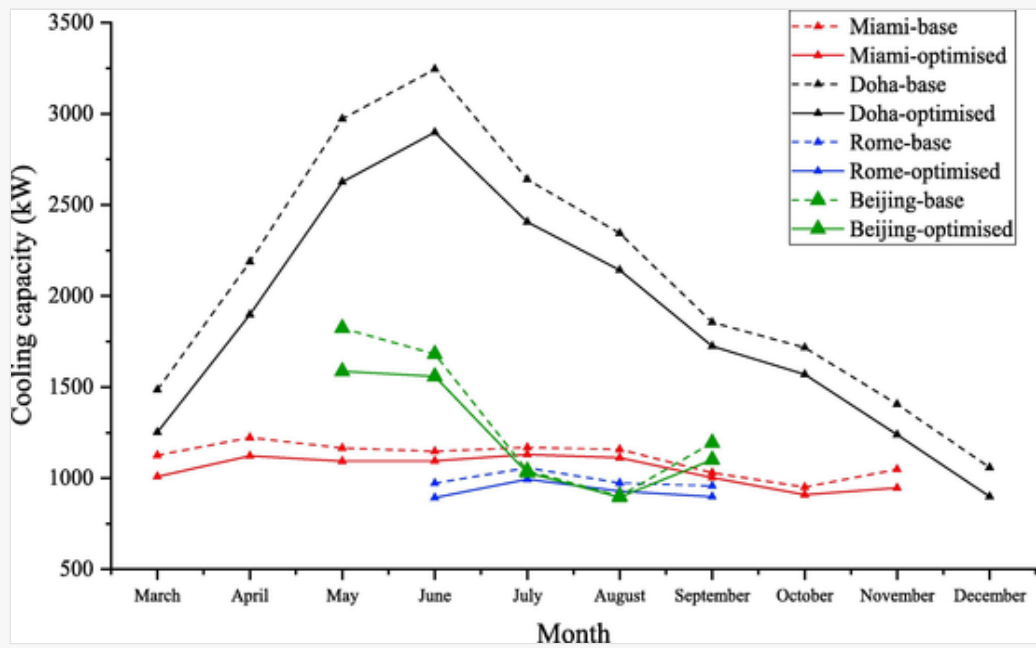
Monthly COP improvement; (a): Miami; (b): Doha; (c): Rome; (d): Beijing.

Fig. 7



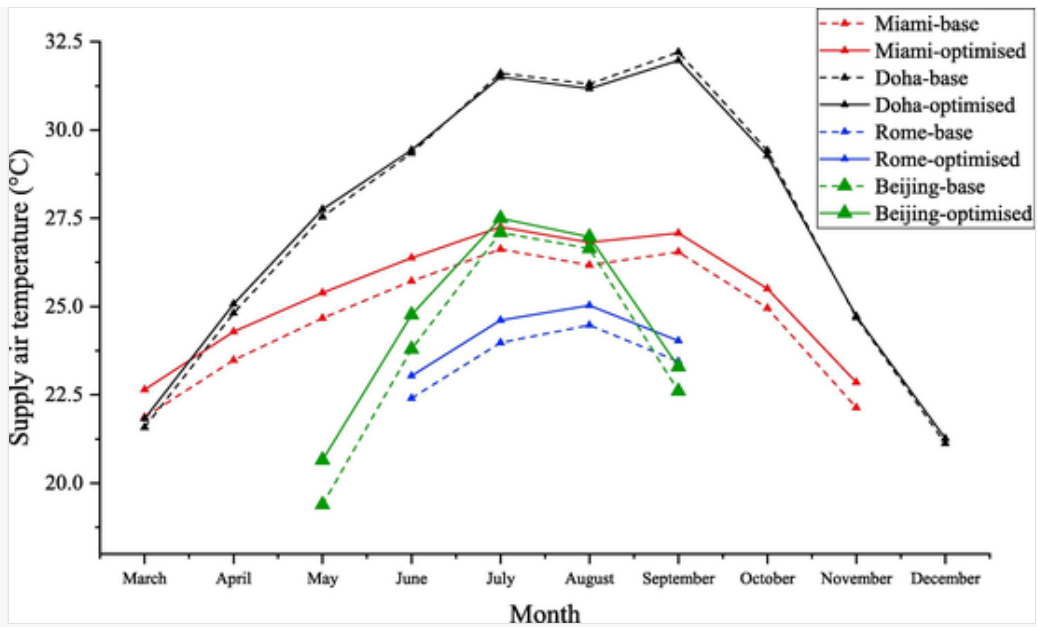
Surface are improvement comparison between the base and optimised conditions.

Fig. 8



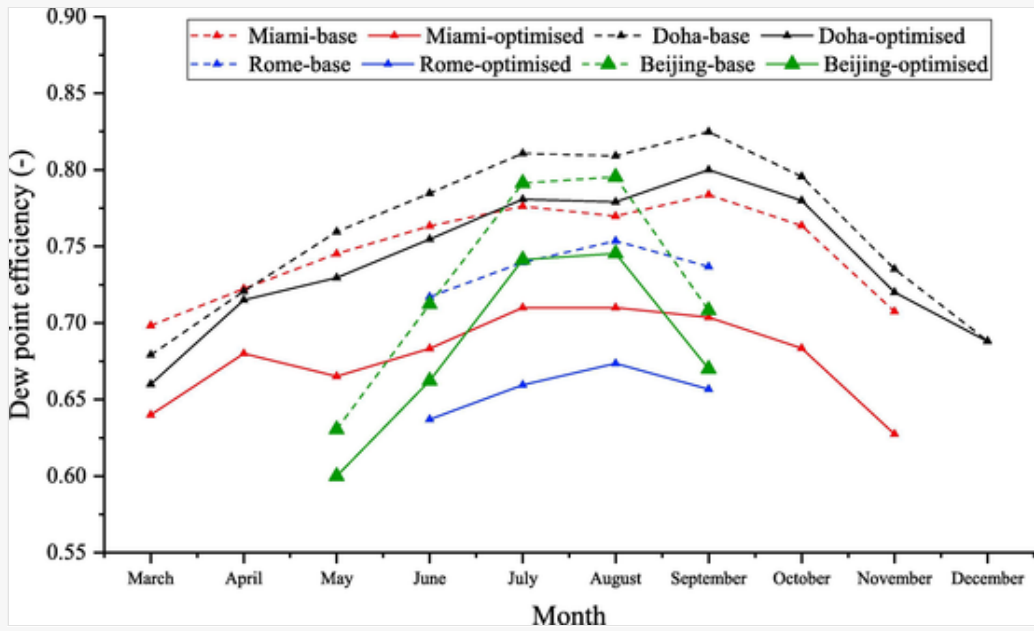
Monthly cooling capacity comparison between the base and optimised conditions.

Fig. 9



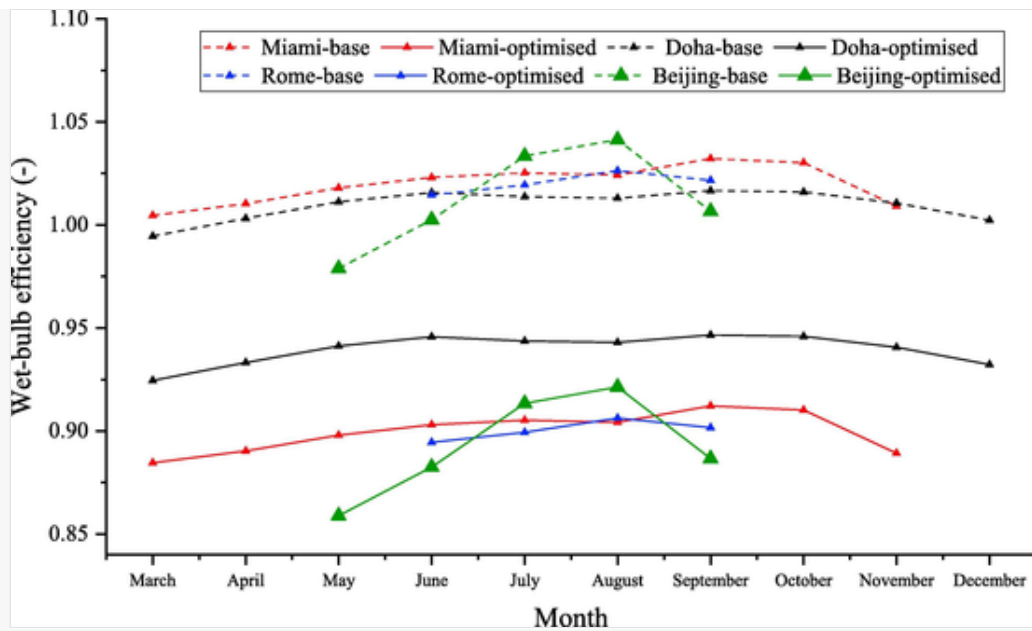
Monthly supply air temperature comparison between the base and optimised conditions.

Fig. 10



Monthly dew point efficiency comparison between the base and optimised conditions.

Fig. 11



Monthly wet-bulb efficiency comparison between the base and optimized conditions.

4.5.1 Monthly investigation

Due to the relatively stable weather conditions in Miami, i.e., the temperature is in the narrow range of 26–31 °C and the relative humidity is in the range of 0.69–0.76, it is expected to have a similar performance in all operating months. The monthly COP under the base and optimum conditions for Miami are shown in Fig. 6(a) in which the COP of the base system was varied from 8.01 in October to 10.34 in April, whereas under the optimum conditions the COP ranges from 26.42 in October to 32.67 in April. Similarly, as shown in Fig. 7, the surface area has decreased in the optimum condition. The surface area of the base system was 62.49 m² whereas it has reduced by 23.57% to 50.57 (m²) in the optimum condition. This is mainly because of the significant reduction in height of the HMX which was 3 (m) in the base condition and has got the lower value of 0.80 (m) in the optimum system. However, the cooling capacity, wet-bulb and dew point efficiencies and supply air temperature are almost unchanged. Fig. 8 shows the cooling capacity of the system in both base and optimised conditions in which it was in the similar ranges of 0.95–1.22 kW and 0.90–1.12 kW in the base and optimised conditions respectively. Similarly, as seen in Fig. 9, the supply air temperature of the base and optimum conditions is in the close ranges of 21.86–26.62 °C and 22.64–27.25 °C respectively. Consequently, the similar behaviour can be seen for the wet-bulb and dew point efficiencies where, as seen in Figs. 10 and 11, the dew point and wet-bulb efficiencies have decreased of up to 11.94% and 11.45% respectively. Although a remarkable improvement has been recorded after the optimization but due to the humid conditions in all operating months, the negative effects of high relative humidity [18,51] keeps the cooling capacity and COP at lower values. For instance, the maximum values of cooling capacity and COP were recorded in April since it holds the lowest relative humidity. However, the minimum values were recorded in October where it is identified as the wettest month.

Because of the wide temperature and relative humidity ranges in Doha during the operating months, i.e., the temperature varies between 25 °C in December to 42 °C in June and July and the relative humidity is in the

range of 0.41–0.71, unstable performance for GIDPC was recorded over the operating months. For instance, as shown in Fig. 6(b), the COP ranged from 9 in December to 27.25 in June. The reason for unsatisfying behaviour in December is that the GIDPC was operated in temperature of 25 °C in which a low cooling capacity was expected. In addition, the wet condition of this month was another reason for unsatisfying performance. Contrarily, the warmest and driest condition in June is the main reason for the best GIDPC performance in Doha. However, the system performance is remarkably improved under the identified optimum conditions where the best performance of the system was recorded in June by the improved cooling capacity of 76.05. Similarly, it is ascertained that the poor performance of GIDPC in an unfavourable condition (December) can also be improved significantly where the optimized COP were recorded as 23.97. In addition, as seen in Fig. 7, the surface area in Doha has decreased by 22.22% and holds the optimum value of 51.88 (m²). However, Fig. 8 shows the cooling capacity of the system in Doha has slightly decreased where the maximum decrease of 0.34 kW has occurred in June. Similarly, as seen in Fig. 9, the maximum difference between the supply air temperature of the base and optimum conditions in Doha is 0.25 °C which has led to the similar behaviour for the wet-bulb and dew point efficiencies in Doha, as seen in Figs. 10 and 11, where the dew point and wet-bulb efficiencies have decreased of up to 4.41% and 7.03% respectively. Thus, it can be concluded that in Arid climate the DPC can perform ideally in all operating months under the optimum conditions.

Rome, as the representative of the Mediterranean hot summer climate, have a relatively cold and wet climate over the operating months where the temperature and relative humidity are in the narrow ranges of 26–28 °C and 0.73–0.75 respectively. Thus, it was expected to observe an unsatisfactory and similar performance in all months where the COP, as seen in Fig. 6(c), varies from 8.09 in September to 8.91 in July. These performances were expected as the September has the minimum and July has the maximum values of relative humidity. Due to the wet conditions in Rome, it is expected to have more improvement if the intake air is pre-treated by a dehumidifier which will lead to lower humidity levels and higher cooling capacity and COP values. In addition, as seen in Fig. 7, a remarkable decrease of 21.01% in surface area is recorded. But similar to the other cities, as seen in Figs. 8 and 9, the cooling capacity and supply air temperature in Rome are almost unchanged where the maximum difference between the base and optimised conditions of the cooling capacity and supply air temperature in Rome are 0.078 kW and 0.63 °C respectively. Similarly, maximum decrease of 0.08 and 0.12 are seen in dew point and wet-bulb efficiencies as seen in Figs. 10 and 11.

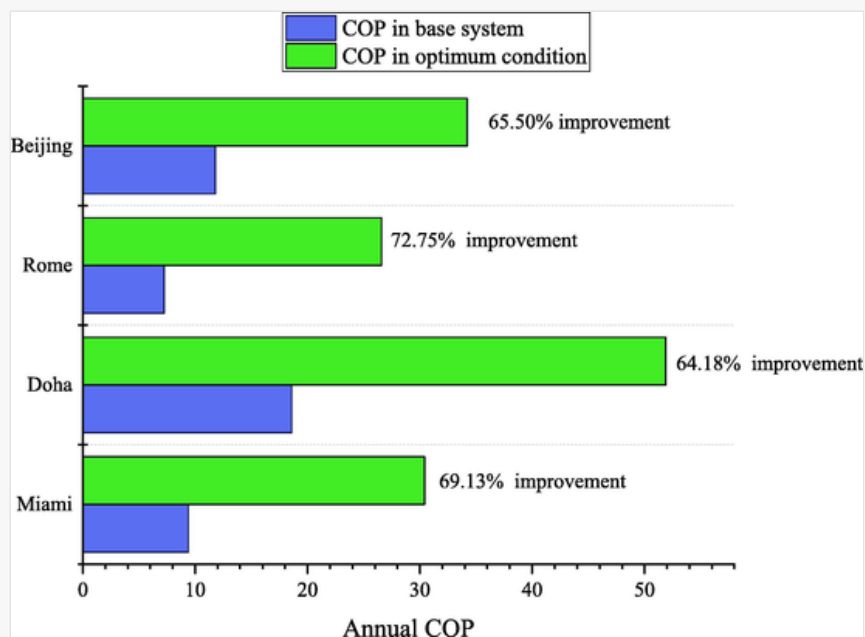
Beijing as the representative of hot summer continental climate, has wet conditions over the operating months except in May where the relative humidity is 0.56 but it ranges from 0.6 in June to 0.78 in August. The temperature also varies from 26 °C in May to 31 °C in July. Based on these values, it can be estimated that the GIDPC will have impermanent performance over the operating months. As can be seen from Fig. 6(d), the COP of the optimum system varies from 24.71 in August to 44.13 in May. The reason for this performance lies in the fact that the wettest condition in August has led to the system's poor performance, and, as expected, the driest condition in May has caused the system to demonstrate its full potential. However, the optimization has increased the system performance substantially where the maximum increase of 28.94 in COP has occurred in June. This means that although July holds the warmest temperature value, i.e., 31 °C, but the base system was not designed properly to demonstrate the full potential of the GIDPC in this month. However, the best performance of the system was recorded in May with the COP value of 44.13. Contrarily, despite remarkable

improvement in system performance, the poorest performance of the system remained in August where the COP is 24.71. In addition, as seen in Fig. 7, the surface area in Beijing has decreased by from 62.75 (m²) to 52.76 (m²) after the optimisation. As seen in Figs. 8 and 9, the cooling capacity and supply air temperature in Beijing are almost unchanged where the maximum difference between the base and optimised conditions of the cooling capacity and supply air temperature in Rome are 0.23 kW and 1.26 °C respectively. Similarly, maximum decrease of 0.05 and 0.12 are seen in dew point and wet-bulb efficiencies in Beijing, as seen in Figs. 10 and 11.

4.5.2 Annual investigation

Having analysed the monthly effects of optimization, it is needed to take the annual figures into account to figure out whether it is worth to have a unique design for the GIDPC in different climates. Thus, the average cooling capacity and COP of the base system and optimum systems in operating months are compared as shown in Fig. 12. In addition, the annual average values of the cooling capacity, supply air temperature, dew point and wet-bulb efficiencies as well as power saving of the GIDPC in optimum conditions which are mainly due to the improved COP and surface area values, are summarized in Table 9. The annual figures are the average values of the monthly values of the performance parameters in each city.

Fig. 12



Annual improvement of COP in all climates.

Table 9

i The table layout displayed in this section is not how it will appear in the final version. The representation below is solely purposed for providing corrections to the table. To preview the actual presentation of the table, please

Annual performance of the system in optimum and base conditions

Representative city	Cooling capacity (kW)		Supply air temperature (°C)		Wet-bulb point efficiency (-)		Dew point efficiency (-)		Power saving (%)
	base	optimised	base	optimised	base	optimised	base	optimised	
Miami	1.11	1.04	24.68	25.35	1.01	0.89	0.74	0.66	43.63
Doha	2.20	1.97	27.36	28.08	1.00	0.94	0.76	0.73	49.41
Rome	0.98	0.92	23.57	24.17	1.02	0.90	0.73	0.65	45.12
Beijing	1.32	1.23	23.90	24.63	1.01	0.89	0.72	0.67	47.33

In Miami, the annual COP of the base system in nine months of operation was 7.24 while it has increased to 26.58 after the optimization. Considering the slight difference between the annual cooling capacity of the base and optimum system i.e., 0.07 kW, and according to the COP equation (Eq. (8)), the optimization has resulted in 43.63% less power consumption. In addition, the difference between the annual supply air temperature, wet-bulb and dew point efficiencies in Miami are 0.67 °C, 0.12 and 0.08 respectively. Similarly, in Doha, the system has operated all along the year except two cold months i.e., January and February. Owing to the relatively warm and dry conditions in Doha, i.e., an average temperature of 35.39 °C and relative humidity of 0.56, the base system performance was better than other climates where the annual COP of the base system was 17.62. However, under the optimized conditions, the annual COP has increased to 51.88. Considering the annual cooling difference between the base and optimised systems i.e., 0.23 kW, power saving of 49.41% is recorded. In addition, the difference between the annual supply air temperature, wet-bulb and dew point efficiencies in Doha are 0.72 °C, 0.16 and 0.07 respectively. But the system has got the worst performance in Rome where the average temperature and relative humidity of the operating months were 27.25 °C and 0.74 respectively. However, the optimization has resulted in 72.75% more COP. The optimisation leads to 45.12% less power consumption over the year. The difference between the annual supply air temperature, wet-bulb and dew point efficiencies in Rome are 0.6 °C, 0.12 and 0.08 respectively. In Beijing, the base system annual cooling capacity and COP over the operating months was 11.24 where it has increased to average value of 34.20 respectively. In addition, considering the slight difference in the annual cooling capacity (0.09 kW), power saving of 47.33% achieved in Beijing. Similar to the other cities, slight decrease can be seen in annual values of supply air temperature, wet-bulb and dew point efficiencies.

5 Conclusion

A constraint multi objective evolutionary optimization using digital twins was developed for the state-of-the-art counter flow dew point evaporative cooler with an innovative guideless irregular heat and mass exchanger (GIDPC). The digital twins was based on the Feed-forward Neural Network (FFNN) and the Multi Objective Evolutionary Optimization (MOEO) was based on Genetic Algorithm (GA) methods. Lack of a robust Artificial Intelligence (AI) model and also a necessity of identifying the optimum operating and design

parameters for GIDPCs were the identified gap through the detailed literature review which is now filled by this study. The digital twins is trained by a comprehensive dataset created by a validated numerical model for a 4-kW GIDPC, and the main optimum operating and design parameters in diverse climates were found. The developed hybrid model was then implemented to demonstrate the monthly and annual GIDPC improvements in all climates. The main outcomes of this study are summarized as follows:

- Out of several weather classifications in Köppen-Geiger climate classifications, four suitable climates i.e., Tropical rainforest climate (Miami), Arid (Doha), Mediterranean hot summer (Rome) and Hot summer continental (Beijing), for the GIDPC operation were detected and the system in the selected warm operating months operation was investigated.
- The FFNN model with four layers were selected as the predictive tool. The input layer which contained seven operating and design parameters, two hidden layers with 45 neurons in each and one output layer which contained five performance parameters of the GIDPC.
- The supply air temperature by FFNN and numerical model was compared to examine the performance of the FFNN model. The results revealed that the predictions made by two models are in good agreement in which the maximum discrepancies between the numerical and NN models in Miami, Doha, Rome and Beijing were 0.32 °C, 0.77 °C, 0.21 °C and 0.54 °C respectively.
- The optimum values of the considered parameters were identified by MOEO for different weight values in which the equally distributed weight values are chosen for the GIDPC performance optimisation.
- The optimum velocity was 2 (m/s) in all climates. Moreover, the working air ratio was in the range of 0.21–0.25, the height and channel gap were in the ranges of 0.80–0.84, 0.005–0.006 respectively while the number of layers holds the same value of 160 in all cities.
- The system operation in the identified optimum conditions revealed that the main improvements are observed in COP and surface area while other performance parameters were almost same. Annual average improvements of up to 72.75% in COP and 23.57% in surface area values are occurred. Consequently, 43.69–47.33% power saving was recorded when the system is designed and operated considering the optimum values.

CRedit authorship contribution statement

Yousef Golizadeh Akhlaghi: Conceptualization, Investigation, Writing - original draft, Writing - review & editing. **Ali Badiei:** Investigation, Writing - original draft. **Xudong Zhao:** Project administration, Funding acquisition. **Koorosh Aslansefat:** Writing - review & editing, Investigation, Conceptualization. **Xin Xiao:** Writing - review & editing, Investigation, Conceptualization. **Samson Shittu:** Investigation. **Xiaoli Ma:** Supervision.


Declaration of Competing Interest

The authors declare that they have no known competing financial interests or personal relationships that could have appeared to influence the work reported in this paper.

Acknowledgement

The authors would acknowledge our sincere appreciation to the financial supports from the European Commission H2020 MSCA programme (for the EU H2020—MSCA-RISE-2016-734340 DEW-COOL-4-CDC project), the National Key R&D Program of China (Grant No. 2016YFE0133300) and UK BEIS project IEEA2021.

References

 The corrections made in this section will be reviewed and approved by a journal production editor. The newly added/removed references and its citations will be reordered and rearranged by the production team.

- [1] Yap C., Cai W., Ooi K., Toh K., Callavaro G., Pillai E. Air-con system efficiency primer: a summary. Singapore: National Climate Change Secretariat and National Research Foundation; 2011.
- [2] Duan Z., Zhan C., Zhang X., Mustafa M., Zhao X., Alimohammadisagvand B., et al. Indirect evaporative cooling: past, present and future potentials. *Renew Sustain Energy Rev* 2012;16(9):6823–6850.
- [3] Pérez-Lombard L., Ortiz J., Pout C. A review on buildings energy consumption information. *Energy Build* 2008;40(3):394–398.
- [4] Kabeel A., Abdelgaied M. Numerical and experimental investigation of a novel configuration of indirect evaporative cooler with internal baffles. *Energy Convers Manage* 2016;126:526–536.
- [5] Anisimov S., Pandelidis D., Danielewicz J. Numerical analysis of selected evaporative exchangers with the Maisotsenko cycle. *Energy Convers Manage* 2014;88:426–441.
- [6] A. Handbook, HVAC systems and equipment: chapter, 1996.
- [7] Caliskan H., Dincer I., Hepbasli A. Exergoeconomic, enviroeconomic and sustainability analyses of a novel air cooler. *Energy Build* 2012;55:747–756.
- [8] Chua K., Chou S., Yang W., Yan J. Achieving better energy-efficient air conditioning—a review of technologies and strategies. *Appl Energy* 2013;104:87–104.
- [9] Glanville P., Kozlov A., Maisotsenko V. Dew point evaporative cooling: technology review and fundamentals. *Ashrae Trans* 2011;117(1):111–118.

[10]

Elberling L. Laboratory Evaluation of the Coolerado cooler indirect evaporative cooling unit, Pacific Gas and Electric Company, 2006.

- [11] Maisotsenko V, Gillan LE, Heaton TL, Gillan AD. Method and plate apparatus for dew point evaporative cooler, Google Patents, 2003.
- [12] Zhao X., Yang S., Duan Z., Riffat S.B. Feasibility study of a novel dew point air conditioning system for China building application. *Build Environ* 2009;44(9):1990–1999.
- [13] Riangvilaikul B., Kumar S. An experimental study of a novel dew point evaporative cooling system. *Energy Build* 2010;42(5):637–644.
- [14] Bruno F. On-site experimental testing of a novel dew point evaporative cooler. *Energy Build* 2011;43(12):3475–3483.
- [15] Jradi M., Riffat S. Experimental and numerical investigation of a dew-point cooling system for thermal comfort in buildings. *Appl Energy* 2014;132:524–535.
- [16] Pandelidis D., Anisimov S. Numerical analysis of the heat and mass transfer processes in selected M-Cycle heat exchangers for the dew point evaporative cooling. *Energy Convers Manage* 2015;90:62–83.
- [17] Lin J., Thu K., Bui T., Wang R., Ng K.C., Chua K. Study on dew point evaporative cooling system with counter-flow configuration. *Energy Convers Manage* 2016;109:153–165.
- [18] Xu P., Ma X., Diallo T.M., Zhao X., Fancey K., Li D., et al. Numerical investigation of the energy performance of a guideless irregular heat and mass exchanger with corrugated heat transfer surface for dew point cooling. *Energy* 2016;109:803–817.
- [19] Xu P., Ma X., Zhao X., Fancey K. Experimental investigation of a super performance dew point air cooler. *Appl Energy* 2017;203:761–777.
- [20] Lin J., Wang R., Kumja M., Bui T., Chua K. Modelling and experimental investigation of the cross-flow dew point evaporative cooler with and without dehumidification. *Appl Therm Eng* 2017;121:1–13.
- [21] Lin J., Bui D.T., Wang R., Chua K.J. On the exergy analysis of the counter-flow dew point evaporative cooler. *Energy* 2018;165:958–971.
- [22] Lin J., Bui D.T., Wang R., Chua K.J. The counter-flow dew point evaporative cooler: analyzing its transient and steady-state behavior. *Appl Therm Eng* 2018;143:34–47.
- [23] Lin J, Wang R, Kumja M, Bui T, Chua KJ. Ecological design and management, “Multivariate scaling and dimensional analysis of the counter-flow dew point evaporative cooler,” vol. 150, pp. 172-187, 2017.

- [24] Lin J, Bui DT, Wang R, Chua KJJAe. On the fundamental heat and mass transfer analysis of the counter-flow dew point evaporative cooler, vol. 217, pp. 126-142, 2018.
- [25] Wan Y, Lin J, Chua KJ, Ren CJEC, and Management, Similarity analysis and comparative study on the performance of counter-flow dew point evaporative coolers with experimental validation, vol. 169, pp. 97-110, 2018.
- [26] Lin J., Huang S.-M., Wang R., Chua K.J. Thermodynamic analysis of a hybrid membrane liquid desiccant dehumidification and dew point evaporative cooling system. *Energy Convers Manage* 2018;156:440–458.
- [27] Wan Y., Lin J., Chua K.J., Ren C. A new method for prediction and analysis of heat and mass transfer in the counter-flow dew point evaporative cooler under diverse climatic, operating and geometric conditions. *Int J Heat Mass Transf* 2018;127:1147–1160.
- [28] Liu Y., Akhlaghi Y.G., Zhao X., Li J. Experimental and numerical investigation of a high-efficiency dew-point evaporative cooler. *Energy Build* 2019;197:120–130.
- [29] Liu Y., Li J.M., Yang X., Zhao X. Two-dimensional numerical study of a heat and mass exchanger for a dew-point evaporative cooler. *Energy* 2019;168:975–988.
- [30] Pandelidis D., Anisimov S. Application of a statistical design for analyzing basic performance characteristics of the cross-flow Maisotsenko cycle heat exchanger. *Int J Heat Mass Transf* 2016;95:45–61.
- [31] Sohani A., Sayyaadi H., Hoseinpoori S. Modeling and multi-objective optimization of an M-cycle cross-flow indirect evaporative cooler using the GMDH type neural network. *Int J Refrig* 2016;69:186–204.
- [32] Jafarian H., Sayyaadi H., Torabi F. Modeling and optimization of dew-point evaporative coolers based on a developed GMDH-type neural network. *Energy Convers Manage* 2017;143:49–65.
- [33] Sohani A, Sayyaadi H, Mohammadhosseini NJEc, and management, Comparative study of the conventional types of heat and mass exchangers to achieve the best design of dew point evaporative coolers at diverse climatic conditions, vol. 158, pp. 327-345, 2018.
- [34] Sohani A., Sayyaadi H., Zeraatpisheh M. Optimization strategy by a general approach to enhance improving potential of dew-point evaporative coolers. *Energy Convers Manage* 2019;188:177–213.
- [35] Pakari A., Ghani S. Regression models for performance prediction of counter flow dew point evaporative cooling systems. *Energy Convers Manage* 2019;185:562–573.
- [36] Lin J., Wang R., Li C., Wang S., Long J., Chua K.J. Towards a thermodynamically favorable dew point evaporative cooler via optimization. *Energy Convers Manage* 2020;203:112224.

- [37] Akhlaghi Y.G., Ma X., Zhao X., Shittu S., Li J. A statistical model for dew point air cooler based on the multiple polynomial regression approach. *Energy* 2019; [181:868–881](#).
- [38] Kottek M., Grieser J., Beck C., Rudolf B., Rubel F. World map of the Köppen-Geiger climate classification updated. *Meteorol Z* 2006;15(3):259–263.
- [39] Handbook AF, American society of heating, refrigerating and air-conditioning engineers, Inc.: Atlanta, GA, USA, 2009.
- [40] Tarkhov D., Vasilyev A.N. Semi-empirical neural network modeling and digital Twins development. Academic Press; 2019.
- [41] Chauvin Y., Rumelhart D.E. Backpropagation: theory, architectures, and applications. Psychology Press; 2013.
- [42] Okut H. Bayesian regularized neural networks for small n big p data. *Artificial Neural Networks-Models Appl* 2016.
- [43] MacKay D.J., Mac Kay D.J. Information theory, inference and learning algorithms. Cambridge University Press; 2003.
- [44] Eiben A.E., Smith J.E. Introduction to evolutionary computing. Springer; 2003.
- [45] Bandyopadhyay S., Saha S. Unsupervised classification: similarity measures, classical and metaheuristic approaches, and applications. Springer Science & Business Media; 2012.
- [46] Elarbi M., Bechikh S., Gupta A., Said L.B., Ong Y.-S. A new decomposition-based NSGA-II for many-objective optimization. *IEEE Trans Syst, Man, Cybernetics: Syst* 2017;48(7):1191–1210.
- [47] Yang XS. “Test problems in optimization,” arXiv preprint arXiv:1008.0549, 2010.
- [48] Zhan C., Zhao X., Smith S., Riffat S. Numerical study of a M-cycle cross-flow heat exchanger for indirect evaporative cooling. *Build Environ* 2011;46(3):657–668.
- [49] <https://weather-and-climate.com>. “Climate and average monthly weather.”
- [50] Chen Y., Yang H., Luo Y. Parameter sensitivity analysis and configuration optimization of indirect evaporative cooler (IEC) considering condensation. *Appl Energy* 2017;194:440–453.
- [51] Akhlaghi Y.G., Zhao X., Shittu S., Badieli A., Cattaneo M.E., Ma X. Statistical investigation of a dehumidification system performance using Gaussian process regression. *Energy Build* 2019; [202:109406](#).

Highlights

- A hybrid model is developed for a novel counter-flow dew point cooler.
 - Digital twins is developed for the system performance prediction.
 - Multi objective optimization is implemented to identify the optimum conditions.
 - Optimum design and operating parameters are identified in four different climates.
 - Performance of the system in the identified optimum conditions is investigated.
-

Queries and Answers

Query: Your article is registered as a regular item and is being processed for inclusion in a regular issue of the journal. If this is NOT correct and your article belongs to a Special Issue/Collection please contact J.Shanmugam@elsevier.com immediately prior to returning your corrections.

Answer: Yes

Query: The author names have been tagged as given names and surnames (surnames are highlighted in teal color). Please confirm if they have been identified correctly.

Answer: Yes

Query: Please specify the significance of bold-italics values cited in the table 4, as a corresponding text has not been provided.

Answer: Having a star beside the Number 9 is enough. Bold-italics are not necessary. The star beside number 9 shows the selected model which is explained in the context.

